JOINT EUROPEAN TORUS JET

JET–P(96)32

Many Authors

JET Invited Papers presented at the 23rd EPS Conference on Plasma Physics and Controlled Fusion

Preprint of Papers to be submitted for publication in Proceedings of the
23rd EPS Conference on Plasma Physics and Controlled Fusion
Kiev, Ukraine, 24th June - 28th June 1996

JET Papers presented at the 23rd EPS Conference on Plasma Physics and Controlled Fusion (Kiev, Ukraine, 24-28 June 1996)

Many Authors

JET-Joint Undertaking, Culham Science Centre, OX14 3DB, Abingdon, UK

Preprint of Paper to be submitted for publication in
the proceedings of the 23rd EPS Conference on Plasma Physics and Controlled Fusion

JET Invited Papers presented at the 23rd EPS Conference on Plasma Physics and Controlled Fusion (Kiev, Ukraine, 24-28 June 1996)

A Review of the Dimensionless Parameter Scaling Studies

by J.G. Cordey, B. Balet, D. Campbell, C.D. Challis, J.P. Christiansen,
C. Gormezano, C. Gowers, D. Muir, E. Righi, G.R. Saibene, P.M. Stubberfield
and K. Thomsen

JET Joint Undertaking, Abingdon, OXON, OX14 3EA U.K.

ABSTRACT

The theoretical basis of the dimensionless parameter scaling technique is derived and the limitations in its application are discussed. The use of the technique is illustrated by the production on JET of steady state ITER similarity pulse having the same β and collisionality as the ignited ITER. The key issue of the scaling of the transport with the main dimensionless parameter ρ^* is discussed in detail. Finally possible shortcomings of the technique are examined.

I. INTRODUCTION

One of the most difficult problems facing the designers of the next generation of fusion experiments is to estimate accurately the energy confinement and fusion performance of a particular design. As yet there is no fully tested 1-D model of the energy particle transport in a tokamak and so one presently has to resort to 0-D global energy confinement projections. Since these don't give the plasma profiles this approach is rather restricted.

An alternative approach which is discussed in this paper is the similarity approach or as it sometimes known the "windtunnel" approach. The basic idea is to design discharges with as many dimensionless parameters as possible at the values that they will have in the next generation of experiments. This can be achieved for all of the dimensionless parameters thought to have an influence on the transport, except the dimensionless Larmor radius parameter $\rho^*(\equiv \rho_i/a)$, where ρ_i is the Larmor radius and a the machine minor radius. Once the dependence of the transport on ρ^* has been determined both by experiments on a single machine and on machines of different sizes, then one can scale the transport coefficient, and as we shall show, the temperature profiles in a simple manner to establish the conditions in a new machine.

The key feature of this similarity approach is that details of the dependence of the transport on quantities such as the safety factor profile q, or the dimensionless profile factor $\eta(\equiv$ DlogT/Dlogn) need not be determined.

The structure of the paper is as follows, in Section II, the theoretical basis behind the technique is presented, then in Section III the JET ITER similarity pulses are described, in Section IV the ρ^* scaling of ELMy H-modes on JET is presented from both a global and local point of view, then in Section V the reasons for completing dimensionless identity experiments are discussed. In Section VI the shortcomings of the technique are examined, and finally in Section VII we examine the connection between global scaling expressions and the ITER similarity pulses.

II. THEORETICAL BASIS OF THE TECHNIQUE

It has been shown by Kadomtsev [1] and Connor and Taylor [2] that the expression for the thermal diffusivity can be expressed in the form

$$\chi = \frac{T}{B} \quad F\,(\rho^*, \beta, \nu^*, q, a/R, \eta, \kappa, \ldots) \qquad (1)$$

provided the turbulence has a scale length larger than the Debye length and the turbulence is not driven by atomic processes.

The smallest of the dimensionless parameters is ρ^* so we can expand in ρ^* without any loss of generality

$$\chi = \frac{T}{B} \quad [\rho^{*-1}\, H\,(\beta, \nu^*, \ldots) + I\,(\beta, \nu. \ldots) + \rho^*\, G(\beta, \nu^*, \ldots)] \qquad (2)$$

The first term in the square brackets describes the loss process arising from free flow along stochastic field lines with a correlation length of order of the minor radius a, the second term is the Bohm term where the turbulence correlation width is of order $\sqrt{\rho_i a}$ and finally the third term is the gyro-Bohm term where the turbulence correlation width is a Larmor radius ρ_i. Most theories of plasma transport are of the gyro-Bohm form, although there are some theories which give rise to Bohm diffusivity. Short MHD events such as sawteeth or ELMs can give rise to stochastic energy loss. Measurements of plasma turbulence in Tokamaks have usually found the correlation width to be of the order of the ion gyro radius supporting the gyro-Bohm theories.

If one of the three terms of equation (2) is dominant across the profile then in principle we do not need to determine its dependence on β, ν^* etc, the value of the function across the profile is sufficient.

In order to keep the dimensionless parameters $\beta(\equiv nT/B^2)$, $\nu^*(\equiv na/T^2)$ and q fixed then the plasma density n, temperature T and current I should scale as follows:

$$n \propto B^{4/3}\, a^{-1/3}$$

$$T \propto B^{2/3}\, a^{+1/3} \qquad (3)$$

$$I \propto Ba$$

$$W \propto B^2 a^3$$

The power and the gas input rate are adjusted to reproduce the above scalings. From Eq. (2) together with ρ^* ($\equiv T^{1/2}/Ba$) $\propto B^{-2/3}\, a^{-5/6}$ the scaling of the thermal diffusivity and the energy confinement time may be derived for discharges satisfying the relations of Eq. (3). For the three different types of transport considered in Eq. (2) we get:

gyro-Bohm	$\chi \propto a^2 B\rho^{*3}$,	$\tau_\varepsilon \propto \rho^{*-3}/B \propto a^{5/2}\, B$	
Bohm	$\chi \propto a^2 B\rho^{*2}$,	$\tau_\varepsilon \propto \rho^{*-2}/B \propto a^{5/3}\, B^{1/3}$	(4)
Stochastic	$\chi \propto a^2 B\rho^{*}$,	$\tau_\varepsilon \propto \rho^{*-1}/B \propto a^{5/6}\, B^{-1/3}$	

Thus the scaling of τ_ε with B is very different for the different types of transport.

III. ITER SIMILARITY PULSES

During the 1995 JET experimental campaign several ITER similarity discharges were set up. With the power that was available (20 MW) it was only possible to reach the β's of the ITER operating point (β_n ($\equiv \beta aB/I$) = 2.3) at fields up to 2T. An example of the time evolution at a steady state ELMy H-mode discharge with the ITER β_n and collisionality is shown in Fig. (1a), and the density and temperature profiles are shown in Fig. (1b). The left hand ordinate in all of the graphs is the JET value of the parameter and the right hand ordinates show the scaled ITER values obtained from Eq's (3) and (4). For the power a gyro-Bohm scaling has been assumed in the graph giving about 80 MW. With the projected α power of 300 MW minus Bremsstrahlung of 110 MW ignition would be easily achieved. If a Bohm scaling is assumed then the required power would be over 600 MW, and only driven operation would be possible with Q around 4. Thus we see that it becomes crucial to determine the scaling of the transport with ρ^*.

IV. THE P* SCALING OF ELMY H-MODES

The first experiments on the ρ^* scaling of ELMy were completed on DIII-D [3], where the confinement both globally and locally was found to have a gyro-Bohm scaling. Similar experiments on JET at 1MA/1T and 2MA/2T also showed a gyro-Bohm scaling [4]. The pulse

characteristics for the two pulses are reproduced in Figs. 2a) and b) and a summary of the global confinement characteristics is given in Table 1. From the table one can see that the density and stored energy are in the correct ratio so the two pulses form a similarity pair according to equation (3). The confinement scales as the toroidal field B indicating a gyro-Bohm confinement.

Table I

Pulse no.	B(T)	1 (MA)	$\langle n_e \rangle / 10^{19}$ M-3	P(MW)	W_{th}(MJ)	τ_{th}
35171 (25.8s)	1	1	2.2	5.03	0.85	0.17
35156 (16.1s)	2	2	5.5	9.47	3.2	0.35

A full local transport has been completed for both these pulses using the TRANSP code. The ratio of the χ's of the 2T and 1T pulses are shown in Fig. (3) normalised to the Bohm scaling. The χ_{eff}'s have been calculated in the same manner as Perkins et al [5].

$$\chi_{eff} = q/(n_e T_e - n_i T_i)/a$$

where q is the total conducted heat flux. This Figure shows that the transport is gyro-Bohm across the profile.

V. DIMENSIONLESS IDENTITY EXPERIMENTS

To confirm that the dimensionless parameter technique is valid and that there are no other important parameters involved in the confinement then ρ^*, β, ν^*, q etc, a series of dimensionless identity experiments have been carried out between JET and DIII-D. In these experiments one attempts to keep all of the dimensionless parameters fixed, including ρ^*. These are really truly analogous to windtunnel experiments in that the engineering parameters are different between the two experiments, and all the dimensionless physics parameters are the same. From equation (4) it can be seen that whatever form the transport takes the τ_ε should be inversely proportional to B. Other times such as the time between ELMs should also vary as 1/B, if a good profile match has been obtained in the edge region.

The preliminary results which are presented in reference (6) do indeed show that the energy confinement accurately scales as predicted, there is however a larger discrepancy in the scaling of the ELM frequency between the two machines.

VI. POSSIBLE SHORTCOMINGS OF THE TECHNIQUE

There are two possible shortcomings of the similarity approach. The first is if the dominant transport process were to change with ρ^*, i.e. with machine size; an example of this is confinement near the L-H threshold. The second is that the effects of profile mismatches on predictions are not easy to estimate. An example of how a small profile mismatch in the edge region has a dramatic effect on the confinement is given at the end of this section.

(a) Confinement in the vicinity of the H-mode threshold

A pair of similarity discharges at higher toroidal fields (1.7T and 3T) than the pair presented in Table I were obtained during the 1995 campaign. The main parameters for these pulses are listed in Table II, from the ratio of confinement times of the two pulses it can be seen that there is no dependence on toroidal field, thus from Eq. (4) the scaling of the confinement is much worse than gyro-Bohm being between Bohm and Stochastic.

Table II

Pulse no.	B(T)	1 (MA)	$\langle n_e \rangle / 10^{19}$ M-3	P(MW)	Wth	τth
33140 (16.6s)	1.7	1.6	3.6	6.6	2.3	0.35
33131 (15.6s)	3	2.8	7.6	21	7.3	0.35

Examination of the local transport for these two pulses Fig. (4) shows that the degradation in the transport of the high field pulse relative to the lower field pulse is in the edge region. The excess power loss is thought to be due to the ELMs.

A rough calculation of the power lost by the ELMs in the high field pulse is approximately 1/3 of the input power. In the absence of this loss, the energy confinement would revert to gyro-Bohm.

The reason that the ELM loss is relatively more significant in the high field pulse is thought to be due to the fact that the power level in this pulse is quite close to that of the L-H threshold, and after each ELM the pulse goes back to L-mode. This conjecture however needs to be confirmed by further experiments.

(b) Sensitivity of confinement to the edge profile

During the ρ^* scaling experiments the same stored energy was obtained in two discharges with different gas fuelling rates; medium and high. However to achieve the same stored energy the power had to be increased from 9 MW in the medium fuelled discharge to 12.5 MW in the high

gas fuelled discharge, reducing the confinement time by some 40%. Indeed if one further increases the fuelling rate one can reduce the energy confinement even further and push the discharge back into the L-mode state [7].

The time development of the two pulses is shown in Fig. 5. The basic global parameters, such as the stored energy and density are essentially identical, however the ELM frequency is some 4 times higher in the strongly fuelled pulse. A close inspection of the profiles in the edge region, see Fig. 6, reveals a slightly broader density profile in the high gas fuelled pulse.

Thus we see that relative small changes in the profile in the edge region strongly affect the nature of the ELMs and also the global energy confinement time. These two effects may not be directly connected in that it is not clear that the energy loss by the ELMs accounts for the change in confinement in this case. However the key point here is that to produce perfectly matched similarity pulses one should also endeavour to scale all particle source rates in the appropriate manner.

VII. COMPARISON WITH GLOBAL SCALING EXPRESSIONS

It is interesting to compare the energy confinement in these ITER similarity pulses and ρ^* scans with the existing global scaling expressions which are being used to predict the performance of ITER. The dimensionally correct form of the ITERH93P scaling, which satisfies the gyro-Bohm constraint, expressed in engineering variables has the form,

$$\tau_{\varepsilon th}^{ITERH93P'} = 0.031\, I^{1.05}\, B^{0.36}\, n_e^{0.21}\, A^{0.38}\, R^{1.86}\, \varepsilon^{-0.14}\, \kappa^{0.65}\, P^{-0.69} \qquad (5)$$

This is very close to the precise ITERH93-P scaling which is

$$\tau_{\varepsilon th}^{ITERH93P} = 0.036\, I^{1.06}\, B^{0.32}\, n^{0.17}\, A^{0.41}\, R^{1.79}\, \varepsilon^{-0.11}\, \kappa^{0.66}\, P^{-0.67} \qquad (6)$$

In Fig. (7) the dimensionless confinement time $B\tau_\varepsilon$ is shown versus the product of B and the scaling expression of eq. (5). All the data except the high gas fuelled are within 13% of the scaling expression. The high gas fuelled pulse is some 40% below the scaling expression. Mixing this type of pulse with lower gas fuelled pulses may be one of the reasons for the large data scatter in the ITER ELMy data base. Thus it is important that the pulses in the data base are characterised with respect to this parameter.

ACKNOWLEDGEMENTS

The authors gratefully acknowledge many useful discussions with T.C. Luce and C.C. Petty of General Atomics.

REFERENCES

(1) B.B. Kadomtsev, Sov. J. Plasma Phys. 1 295 (1975).
(2) J.W. Connor and J.B. Taylor, Nucl. Fusion 17, 1047 (1977).
(3) C.C. Petty, T.C. Luce, K.H. Burrell et al. Physics of Plasmas Vol. 2, 2342 (1995).
(4) B. Balet, et al. Proceedings EPS Conference Bournemouth (1995).
(5) F.W. Perkins, et al. Phys. Fluids B **5** (1993) 477.
(6) C.C. Petty, et al. EPS Kiev 1996.
(7) G. Saibene, et al. PSI Conference 1996.

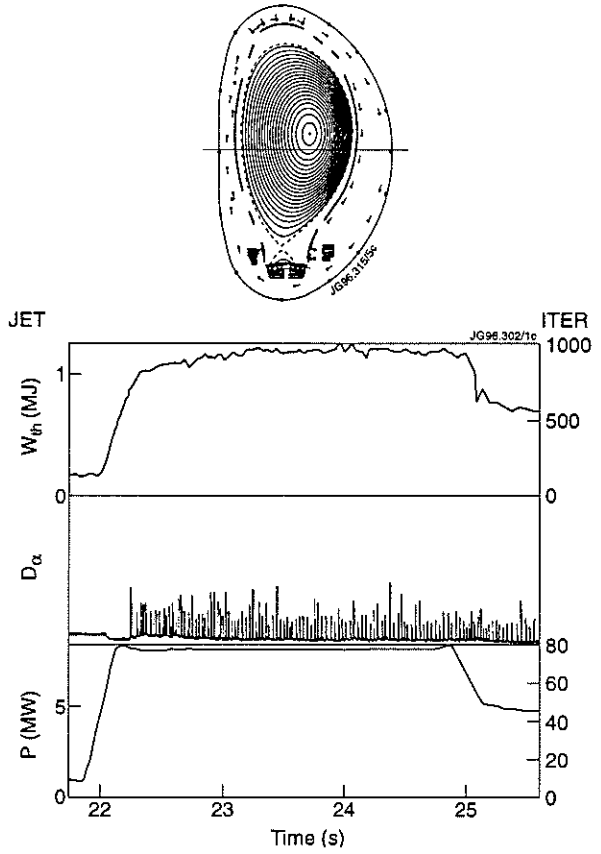

Fig. 1 (a) Thermal stored energy, D_α trace and total input power versus time. The left hand axis is the JET pulse 35174 (β_{nth} = 2.3, $q_{\psi 95}$ = 3.2), the right hand axis are the scaled ITER values.

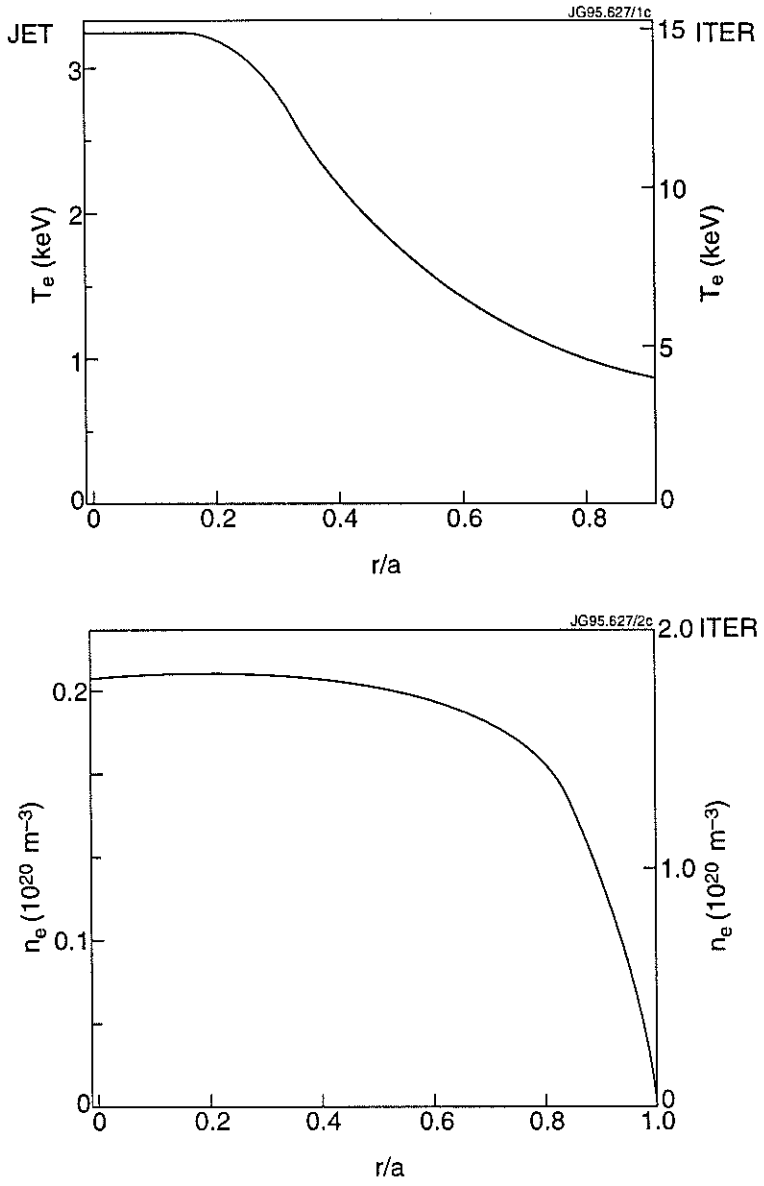

Fig. 1 (b) The temperature and density profiles of pulse 35174, the left hand axis are the JET values, the right hand axis are the scaled ITER values.

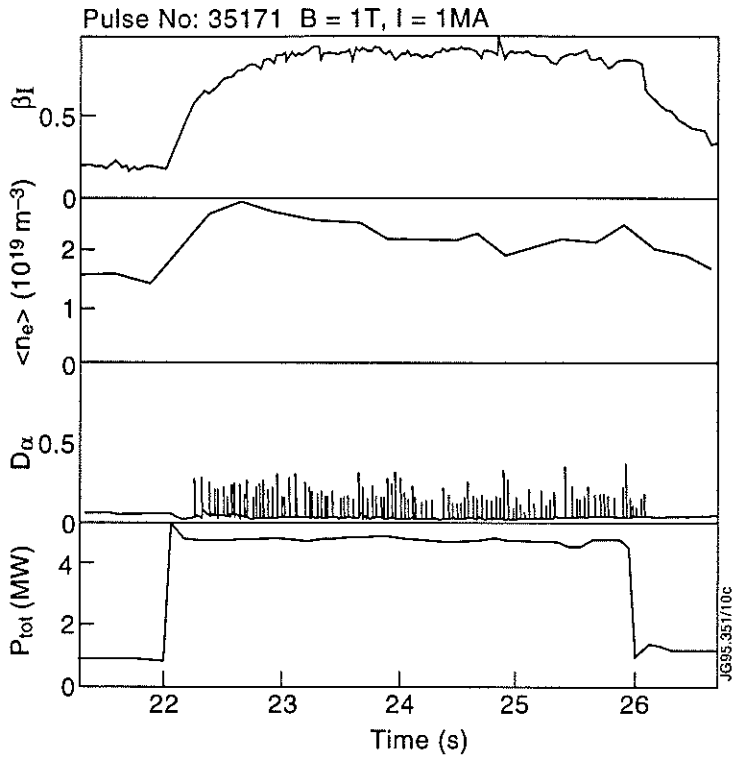

Fig. 2 (a) Time development of the 1MA/1T pulse 35171, β_n, volume average density, D_α and total input power.

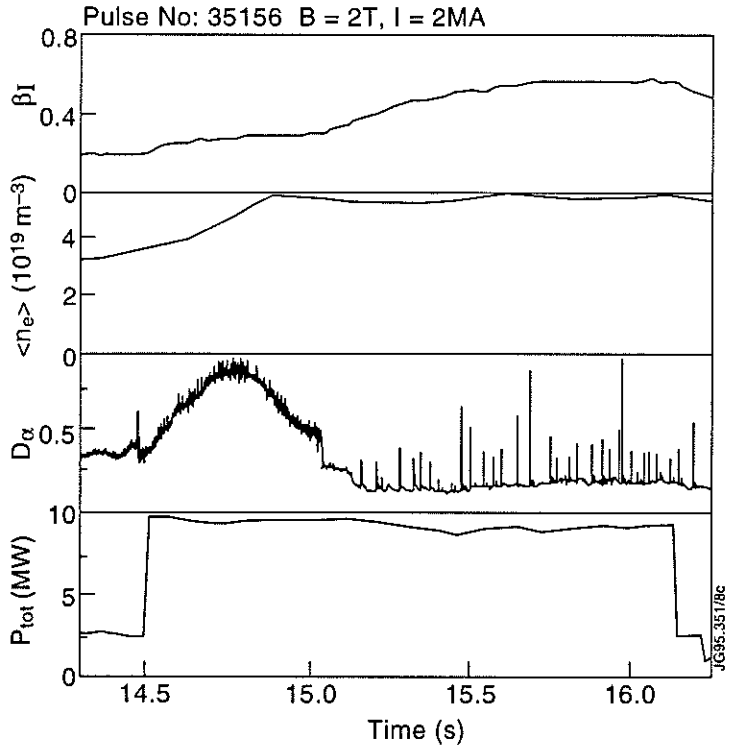

Fig. 2 (b) Time development of the 2MA/2T pulse 35156, β_n, volume average density, D_α and total input power.

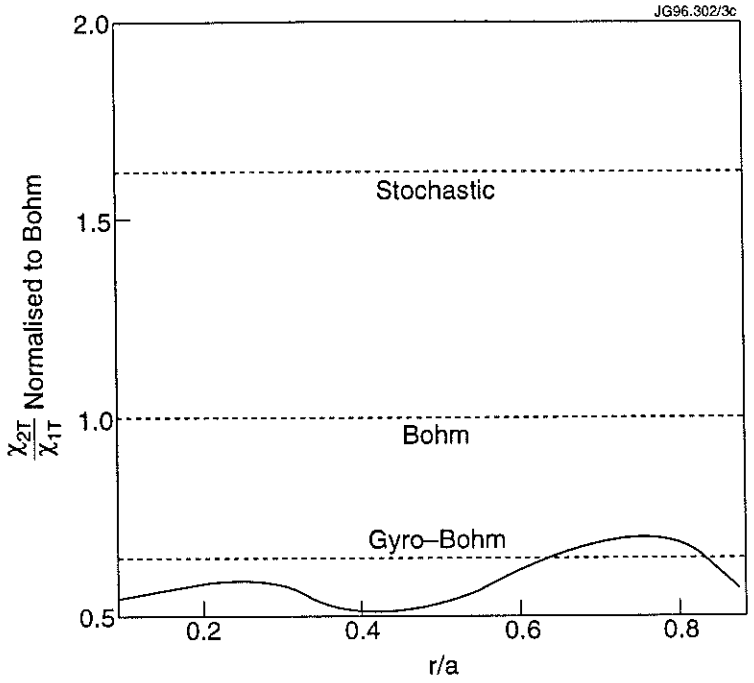

Fig. 3. Ratio of the χ_{eff}'s of the 2T pulse (35156) to the 1T pulse (35171) normalised to Bohm versus the normalised radius r/a.

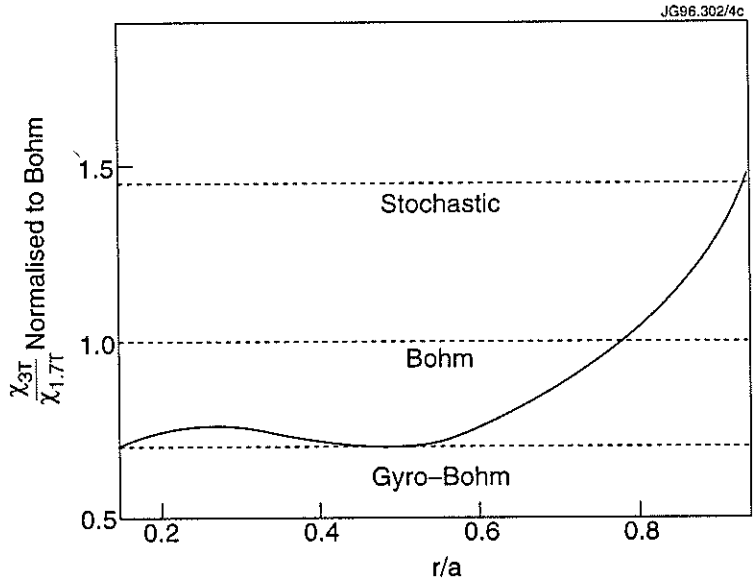

Fig. 4. Ratio of the χ_{eff}'s of the 3T pulse (33131) to the 1.7T pulse (33140) normalised to Bohm versus the normalised radius r/a.

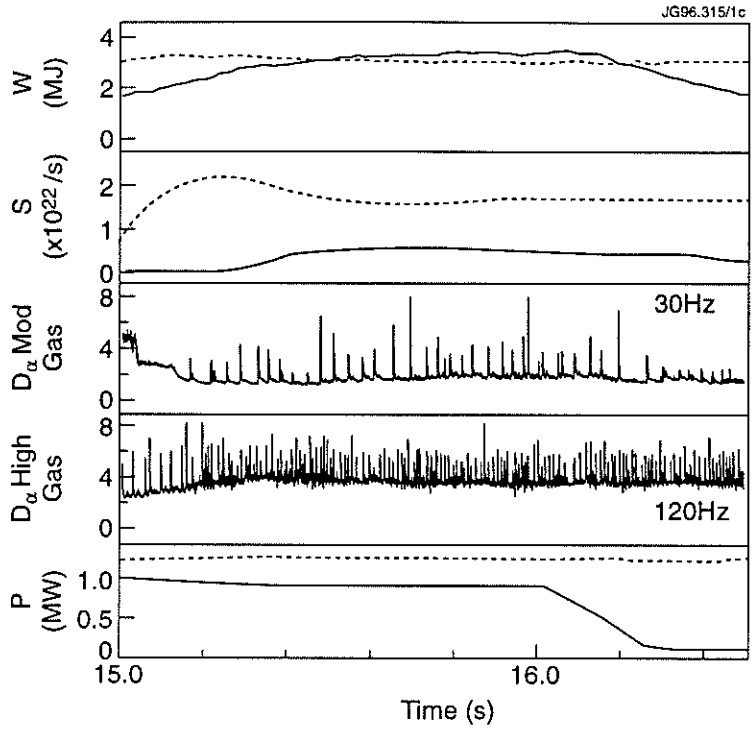

Fig. 5. Stored energy, gas fuelling rate, D_α for low fuelling pulse (35156), D_α for high fuelling pulse (35176), total input power versus time. The dotted curve is the high gas fuelled pulse (35176), the continuous line is for the low fuelled pulse (35156).

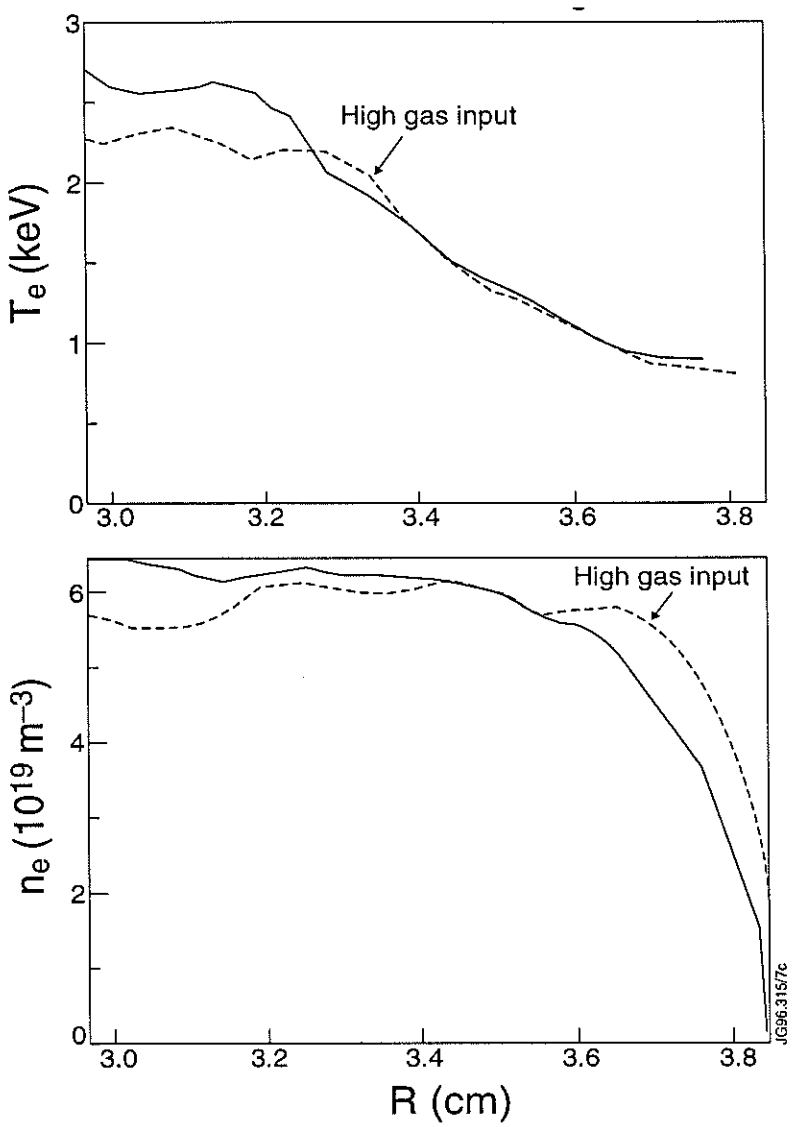

Fig. 6. Temperature and density profiles for the two pulses (35156, 35176) versus normalised radius.

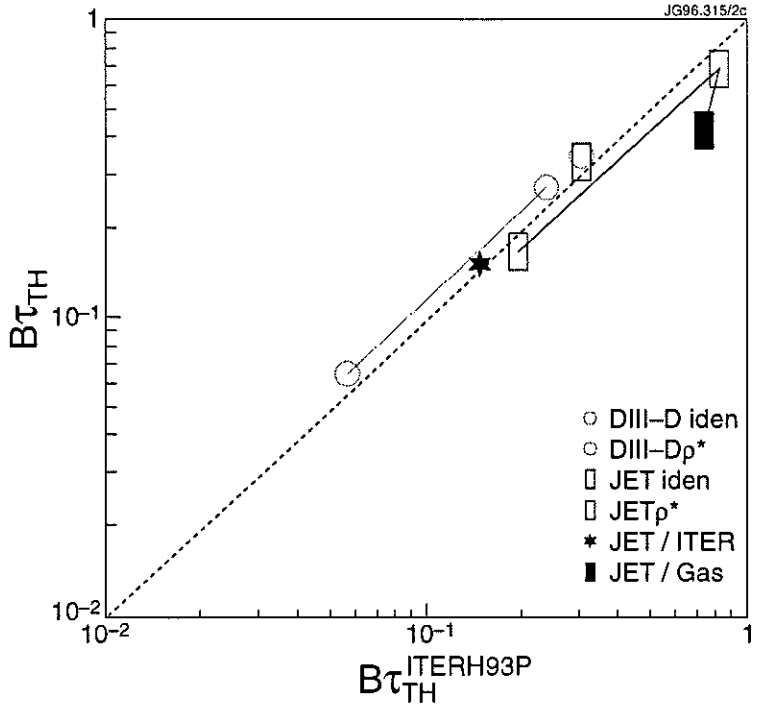

Fig. 7. The dimensionless thermal confinement time versus the product of the scaling expression of equation (5) and the toroidal field. The JET points are the ρ scan described in Section IV, the ITER similarity pulse is from Section III, the high gas input pulse is from Section V, the DIII-D ρ* scan was from Reference III, and the JET /DIII-D identity pulse is from T. Luce (private communication).*

High Density Divertor Operation in JET

L.D. Horton, the Divertor Task Force and the JET Team

JET Joint Undertaking, Abingdon, OXON OX14 3EA, U.K.

ABSTRACT.

Operating the JET Mark I divertor at high density and with high volume losses is shown to have many beneficial effects on divertor performance. On the other hand, combining high density operation with high confinement (H-mode) operation is difficult. In particular, the density at which the plasma naturally operates in ELMy H-mode discharges is difficult to vary. A scaling for how this natural density depends on toroidal field, plasma current, and input power suggests that high density may be achievable in reactors but requires a dedicated multi-machine database, in particular to verify size scalings. Experiments with and without active pumping in the divertor show that the confinement varies with the neutral pressure in the main chamber rather than the fuelling rate *per se*, making operation with a closed divertor attractive. Such a divertor, Mark IIA, has recently been installed in JET and is now operational. First results are presented demonstrating that the operating regimes relevant to JET's programmes have been re-established.

1. INTRODUCTION

A significant part of the experiments aimed at exploiting the Mark I divertor in JET was done in conditions of high density and high volume losses. There are several complementary justifications for this emphasis. The fusion yield in a reactor will scale with the square of the plasma density. The design, for example, of the International Tokamak Experimental Reactor (ITER) relies on operating at high density ($\langle n_e \rangle = 1.3 \times 10^{20} m^{-3}$) in order to achieve ignition [1]. Present day machines tend to operate up to a maximum density described by the Greenwald limit [2]:

$$\langle n_e \rangle^{max} \left[10^{20} m^{-3} \right] = \frac{I_p}{\pi a^2} \qquad (1)$$

where I_p is the plasma current in MA and a is the plasma minor radius in m. The Greenwald density limit for ITER is $0.8 \times 10^{20} m^{-3}$, a value for which the machine would not ignite in standard H-mode conditions.

In addition to the question of fusion yield, operating at high density is necessary in a reactor in order to maximise the volume losses from the plasma edge and scrape-off layer (SOL)

and so protect the divertor target tiles from heat loads in excess of 5 MW/m^2. Finally, by operating at sufficiently high volume losses, it is possible to cool the divertor plasma to less than 5 eV at which point the flow of ions to the plates is reduced (divertor detachment) thus alleviating problems of target erosion.

2. THE H-MODE DENSITY LIMIT

During the Mark I operating campaign the highest density achieved in ELMy H-mode plasmas closely followed the Greenwald scaling. Only at the lowest current (1 MA) was the Greenwald value exceeded and then by 10-20%. This density limit is not disruptive however, and is thought to be due to a completely different mechanism than the normal, disruptive limit found in Ohmic and L-mode plasmas. The behaviour of the plasma density and confinement in ELMy H-modes as the gas fuelling rate is increased is shown in Fig. 1. It can be seen that the density rises only marginally with external fuelling and that the confinement degrades smoothly (no sharp back transition) until, at the highest fuelling rates, the plasma reverts to L-mode. The ELM behaviour changes dramatically as the fuelling level is increased. In unfuelled discharges the ELMs are large discrete events as measured by D_α emission from the divertor. As the fuelling is increased the ELM frequency also increases and their amplitude, as measured in D_α light, decreases until, at the highest gas flows in this experiment, the plasma makes a transition back to L-mode and the ELMs disappear.

By studying the confinement of ELMy H-modes with the divertor cryopump on and off in separate discharges, it is possible to compare similar discharges with very different fuelling rates. Such a comparison is shown in Fig. 2. It can be seen from Fig. 2(a) that significantly higher densities were accessible with the cryopump on. Discharges reaching or exceeding the Greenwald limit were only possible in these cases where the neutral gas pressure in the vacuum vessel is controlled by the cryopump. Furthermore, the confinement of ELMy H-mode discharges appears to depend directly on the main chamber pressure (Fig. 2(b)) rather than the fuelling rate *per se*, both for the cases with cryopump on and off. It is this degradation of performance with main chamber pressure which effectively sets the H-mode density limit in JET.

3. SCALING OF THE NATURAL DENSITY IN JET

As was discussed in the previous section, it is difficult to vary the density of an ELMy H-mode due to the decreased particle confinement (increased ELM frequency) as gas is added. In fact, in dedicated experiments relying not only on fuelling rate but also on varying the pumping speed it is only possible to achieve a 50% variation of the plasma density. It is thus important to understand and be able to scale the density at which an ELMy H-mode naturally operates. For

the purposes of such scaling experiments, the 'natural' density is defined as that which is reached in quasi-steady state with beam fuelling, but no external gas puffing, in a standard configuration centred on the horizontal plates of the Mark I divertor. A data set of such discharges was assembled covering a range of plasma currents from 1 to 3 MA, of toroidal field from 1 to 3 T, and of input power from 5 to 15 MW. A regression of the density of these discharges against plasma current, toroidal magnetic field, and input power is shown in Fig. 3. In fact, only a few points in this data set have a q significantly different from 3, so the toroidal field and plasma current are strongly correlated. If one eliminates the B-dependence by assuming a constant q, the natural density in JET ELMy H-modes scales roughly as the square root of the product of the plasma current and the input power. This power dependence is potentially very important when trying to predict the natural operating density of ITER. If one assumes the same size scaling as in the Greenwald limit, i.e.

$$\langle n_e \rangle \propto \frac{\sqrt{I_p P_{add}}}{\pi a^2}$$

and then scales from the densities obtained in JET, one would expect ITER to operate naturally at $\approx 1 \times 10^{20} m^{-3}$, already 20% above the Greenwald limit and within 30% the required operating point.

4. HIGH DENSITY OPERATION WITH IMPURITY SEEDING

In addition to operating at high density, it is possible to increase the volume power losses from the plasma by seeding the discharge with an impurity. In this way, it is possible to reduce the power loading on the divertor target tiles by an order of magnitude while still maintaining H-mode behaviour, if at somewhat reduced confinement [3]. The price which is paid in this scenario is an unacceptably high Zeff in the plasma core (Fig. 4), which depends on which seed impurity is used. For comparison, the Zeff required for ITER (excluding the contribution of helium ash) is 1.2. It is thought that the large range of Zeff in the neon discharges shown in Fig. 4 is due to insufficient simultaneous deuterium fuelling in many of the neon discharges which were performed before the recipe for radiative discharges was optimised.

It is difficult to extrapolate the results of these radiative experiments to the reactor regime where plasma surface to volume ratios, for instance, will be more favourable. In order to provide some basis for such an extrapolation, a multi-machine database of such discharges was established. Analysis of this database was reported in detailed by Matthews et al. at this year's Plasma Surface Interaction meeting [3] but the important conclusion for the discussion of high density operation here is the strong dependence found on density across all the machines (Fig. 5). Because ITER intends to operate at very high density, it should be possible to radiate large amounts of power for relatively low impurity concentrations. Thus, the problem of power

handling of the divertor target plates, at least in the absense of large ELMs, seems to be primarily a question of operating at sufficiently high densities. Unfortunately, radiating discharges in particular seem to be difficult to operate at high density. In JET, radiative discharges typically operate at 70% of the Greenwald limit, perhaps due to reduced particle confinement in these regimes which have high ELM frequencies. These densities are typical of the different machines in the radiative database.

5. DETACHMENT AND EROSION CONTROL

Another advantage of operating with high divertor density and thus at low divertor temperature is demonstrated in Fig. 6. As the core density is raised during this pulse the divertor temperature drops to the point where collisions between ions in the SOL and recycling neutrals begin to carry away a significant fraction of the ion momentum. This manifests itself as a pressure drop along the SOL from the upstream values next to the core plasma to the target, the divertor detachment regime. The pressure drop along the field lines is maximum near the separatrix and can be larger than a factor of 10, as shown in the Ohmic pulse in Fig. 6. When there is such a pressure drop the flux of ions reaching the divertor target is significantly reduced and thus the erosion of the target is also reduced. Careful studies of the profile of the ion flux to the target [4] show that only on the inner leg of the divertor is there a significant drop of the total flux of ions to the target, integrated over the whole target profile. On the outer leg the peak value of the ion flux drops, but the integral remains roughly constant. This behaviour has been modelled using the EDGE2D two-dimensional fluid code [5] and can be reproduced only if recombination is important on the inner (cooler) leg of the divertor. In any case, the peak erosion rate is reduced significantly on both legs. In experiments on beryllium target tiles, the erosion of beryllium drops almost to zero when the divertor detaches [6]. On carbon tiles there is a significant reduction in erosion (>2x in Ohmic discharges) when the divertor detaches with the remaining carbon influx thought to be due to chemical sputtering, primarily by neutrals rather than ions.

The erosion of carbon divertor tiles has been measured for a hot-ion H-mode shot using a colourimetry technique [6]. The result of this experiment is shown in Fig. 7. The net erosion was measured to be 20 nm for this pulse, in agreement with calculations using the DIVIMP impurity transport code [7] only if there is strong local redeposition of carbon on the target plates. In fact, calculations suggest that the chemical sputtering contribution to the net erosion is small due to large, local redeposition of carbon when it is released as low energy hydrocarbon molecules.

6. IMPURITY EXHAUST

The exhaust of impurities from the plasma also benefits from operation at high densities. The pump out of small puffs of neon, used for impurity retention experiments [8], is shown in Fig. 8 for two different core densities. The exhaust rate in these L-mode dishcarges is four times higher at $4.1\times10^{19}\,m^{-3}$ than at $2.9\times10^{19}\,m^{-3}$. Such an increase in exhaust rate may prove to be crucial for the extraction of helium ash from a reactor, which is thought to be limited by pumping speed rather than by core transport in ELMy regimes [9].

Impurity compression in the divertor would alleviate the problems of core Zeff for radiative discharges discussed above. In order to study this, measurements of the nitrogen-to-deuterium neutral gas concentration in the subdivertor volume are compared to the nitrogen concentration in the plasma core, as deduced from Zeff measurements [10]. Enrichment factors, defined as the ratio of these two concentrations, can be as large as 30 during this type of discharge. Unfortunately, spectroscopic measurements of nitrogen emission from the divertor show that such enrichment factors are not achieved between the core and divertor plasmas.

7. THE JET MARK IIA DIVERTOR

JET has recently finished installing and commissioning a new divertor structure, Mark IIA, which is designed to test the effects of a more closed divertor geometry. For comparison the poloidal profiles of the Mark I and Mark IIA divertors are shown in Fig. 9. The Mark II divertor is designed to allow quick and remote interchange of divertor geometries for testing different concepts for ITER. To that end, the divertor is based on a toroidally continuous inconel support structure with the divertor target tiles mounted on carriers which can in turn be remotely installed on the structure. A segment of the Mark IIA divertor was successfully installed using the remote handling equipment in order to test this capability. It will be necessary to remotely install the next divertor geometry in 1997 after the planned D-T experimental campaign.

Initial indications are that the new Mark IIA divertor is more closed than Mark I. This is shown for Ohmic discharges in Fig. 10. The neutral pressure in the subdivertor volume is two to three times larger in Mark IIA as compared to Mark I at the same plasma density. Predictive modelling using EDGE2D also shows a factor of 2 to 3 increase in subdivertor pressure and pumping speed in Mark IIA as compared to Mark I.

In addition to the divertor, another system which underwent major modifications during the shutdown was the ICRH heating system. Both the antennae hardware and the controlling software were modified with the intention of improving reliability, especially during ELMy H-modes. In addition, the poloidal limiters which protect the antennae were reshaped so as to conform better to the antennae profile and thus provide less shadowing between the antennae

and the plasma. These modifications have all been tested successfully with the result that the ICRH system now delivers 10 MW routinely, with coupling essentially independent of the plasma shape and depending only on the gap between the plasma edge and the antennae. Up to 14 MW of ICRH have been injected into X-point plasmas, producing good quality ($H_{ITER-89P}$=2) ELMy H-modes with central electron temperatures of 8 keV.

ELMy H-mode operation has, in fact, been re-established both with ICRH and NBI heating. A comparison of an ELMy H-mode in Mark IIA to an equivalent discharge in Mark I is shown in Fig. 11. In both cases the performance is good, with the same stored energy produced for the same input power. The ELM behaviour appears to be somewhat different and is different in Mark IIA depending on the magnetic configuration used. This is a subject of current investigation.

Finally, ELM-free operation has also been re-established with the Mark IIA divertor. An ELM-free H-mode from the first day of such experiments is shown in Fig. 12. The high performance period is terminated by an ELM almost three seconds after the high power heating is applied. The performance of this discharge is as good as any of the discharges in the Mark I campaign at the same input power (Fig. 13) which bodes well for performance at full power in Mark IIA leading up to the planned tritium operation at the end of the year.

8. CONCLUSIONS

High density divertor operation has been shown to have many advantages for a fusion reactor. Acceptable power loading of the divertor target plates depends on operation at high densities. A significant reduction of target erosion is possible in detached divertor regimes which accompany high density operation. Finally, impurity exhaust is greatly improved at high density.

Unfortunately, it is difficult to operate at high density while at the same time maintaining high core confinement. The density of ELMy H-modes is very difficult to vary in JET and indeed only possible at gas flows rates which are unattractive in a reactor. It is thus perhaps more useful to study the variation with engineering parameters of the density at which one naturally operates rather than concentrating solely on how high the density can be pushed in extreme conditions. How the 'natural' density of JET ELMy H-modes varies with plasma current, input power, and magnetic field has been investigated and suggests a scaling more favourable than the normal Greenwald limit. Nevertheless, the H-mode density limit in present day machines is well described by the Greenwald value and further work is required to verify the true variation of density with input power, plasma current and size.

The new JET Mark IIA divertor has been installed and commissioned. It appears to be more closed to recycling neutrals, as predicted by modelling. Operation in both ELM-free and ELMy H-mode regimes has been re-established with the Mark IIA geometry and compares favourably with the best discharges from Mark I. Operation in deuterium is now planned

through to the autumn of 1996, followed by a period of operation in deuterium-tritium mixtures. Further divertor geometries can now be tested by remotely replacing the carriers on which the divertor tiles are mounted. The next such experiment will be a 'gas-box' geometry similar to the divertor currently being considered for ITER and is planned to be installed in 1997.

REFERENCES

[1] ITER-JCT and Home Teams (presented by G. Janeschitz) 1995 *Plasma Phys. Controlled Fusion* **37** A19-A35

[2] Greenwald, M., et al. 1988 *Nucl. Fusion* **28** 2199-2207

[3] Matthews, G.F., et al., in proceedings of the 12th International Conf. on Plasma-Surface Interactions, St. Raphael (1996) to be published in J. *Nucl. Mater.*

[4] Loarte, A., et al., in proceedings of the 12th International Conf. on Plasma-Surface Interactions, St. Raphael (1996) to be published in *J. Nucl. Mater.*

[5] Taroni, A. et al., *J. Nucl. Mater.* **220-222** (1995) 1086

[6] Guo, H.-Y., et al., in proceedings of the 12th International Conf. on Plasma-Surface Interactions, St. Raphael (1996) to be published in *J. Nucl. Mater.*

[7] Stangeby, P.C. and Elder, J.D., *J. Nucl. Mater.* **196-198** (1992) 258

[8] Harbour, P.J., et al., *Controlled Fusion and Plasma Physics* (Proc. 22nd Eur. Conf. Bournemouth, U.K.), Vol. 19C, Part IV (1995) IV-465

[9] Hillis, D.L. et al., proceedings of the 3rd International Workshop on Helium Transport and Exhaust.

[10] Ehrenberg, J.K., et al., in proceedings of the 12th International Conf. on Plasma-Surface Interactions, St. Raphael (1996) to be published in *J. Nucl. Mater.*

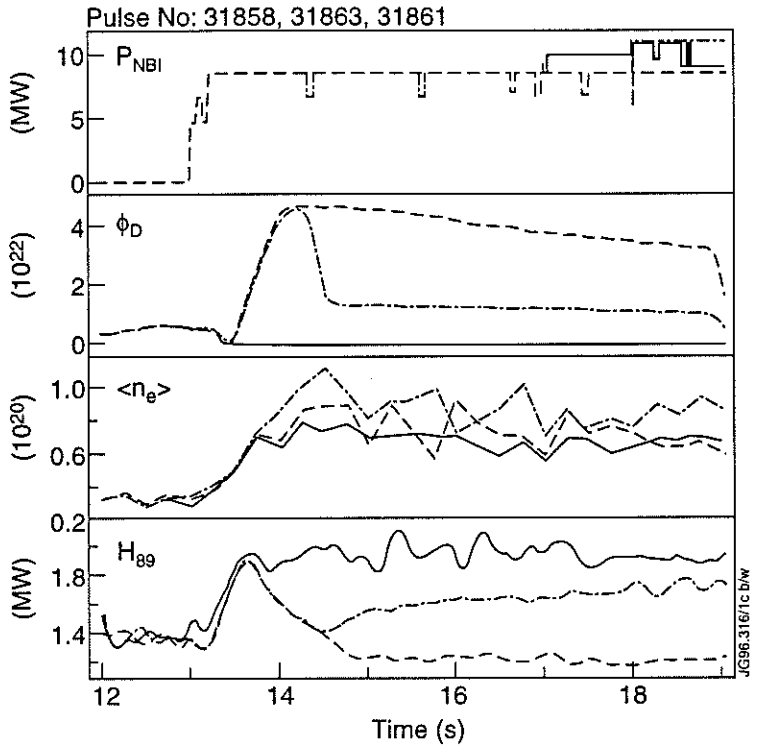

Figure 1: Density limit experiment in ELMy H-mode plasmas at constant input power and for three different deuterium gas fuelling rates: 0 (solid curves), 1×10^{22} atoms/s (dot-dashed curves), and) $\approx4\times10^{22}$ atoms/s (dashed curves). As the fuelling rate is increased, the density only marginally rises before falling again as the confinement drops to L-mode levels.

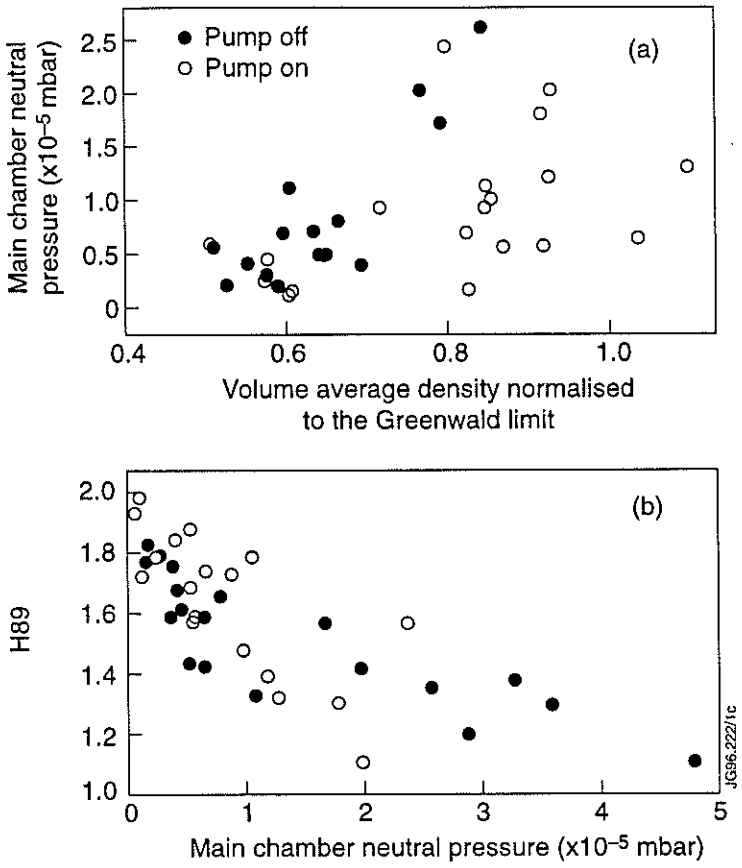

Figure 2: Comparison of the performance of ELMy H-mode discharges with and without pumping in the subdivertor volume. (a) The neutral deuterium pressure measured in the main chamber of the vacuum vessel next to the core plasma versus the volume-averaged density of the plasma. (b) The confinement of the plasma, relative to the ITER-89P scaling versus the main chamber pressure.

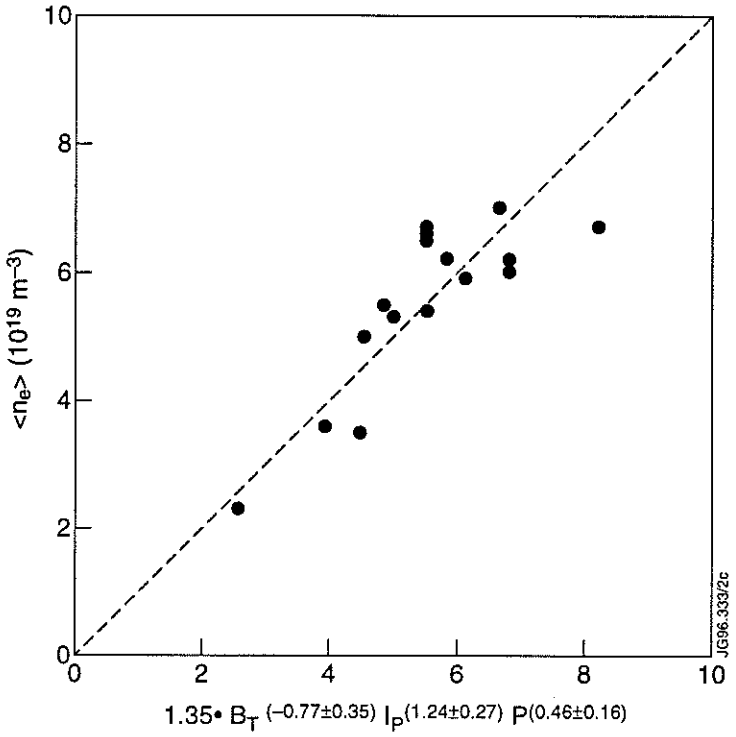

Figure 3: Regression of the volume-averaged density in ELMy H-mode discharges fuelling by neutral beam heating alone against toroidal field [T], plasma current [MA], and input power [MW].

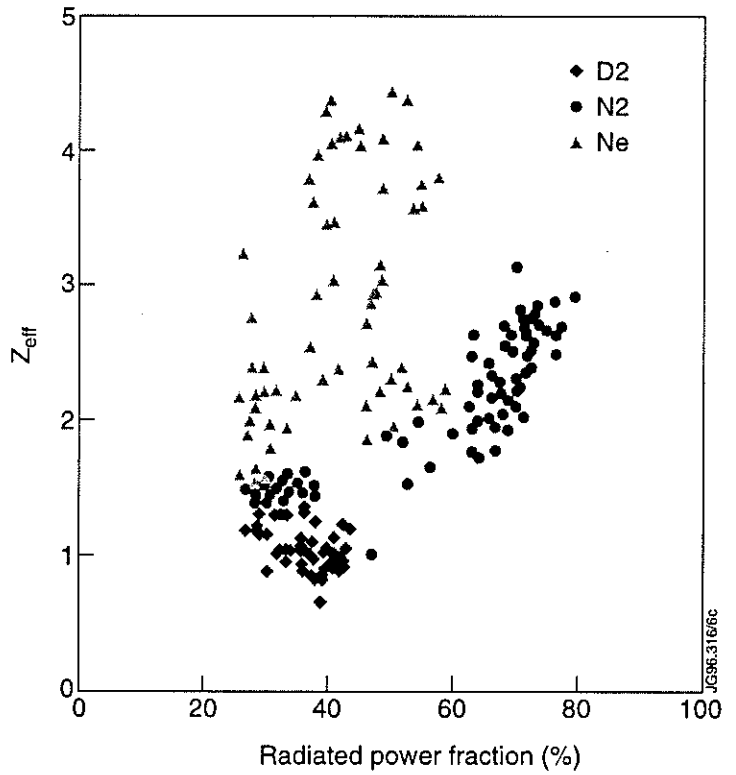

Figure 4: The Zeff of ELMy H-mode plasmas with high radiating power fractions, generated by puffing various extrinsic impurities into the discharge.

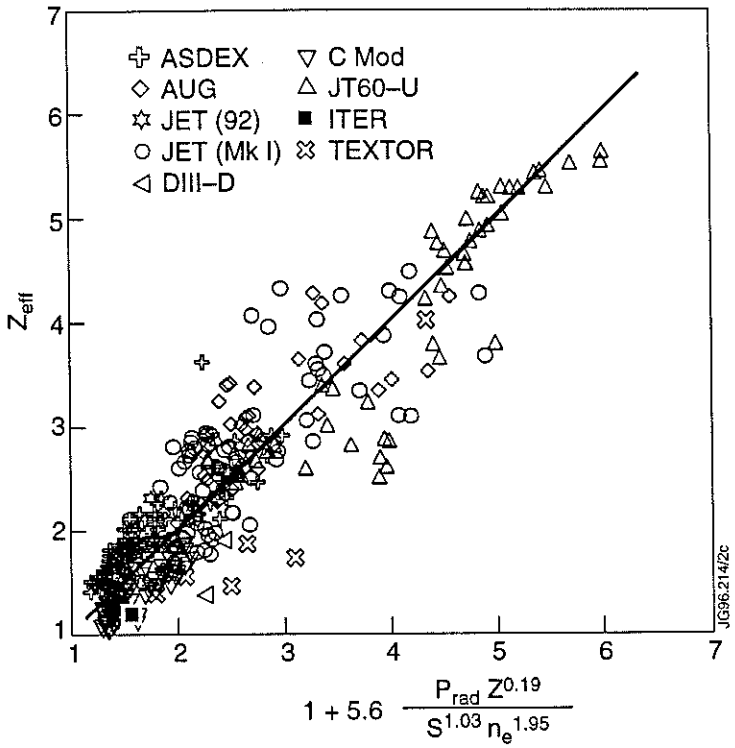

Figure 5: The scaling of Zeff versus input power, plasma surface area, line-averaged density, and impurity atomic number for a multi-machine database as reported in [3]. The operating point for ITER is shown by the solid square for comparison.

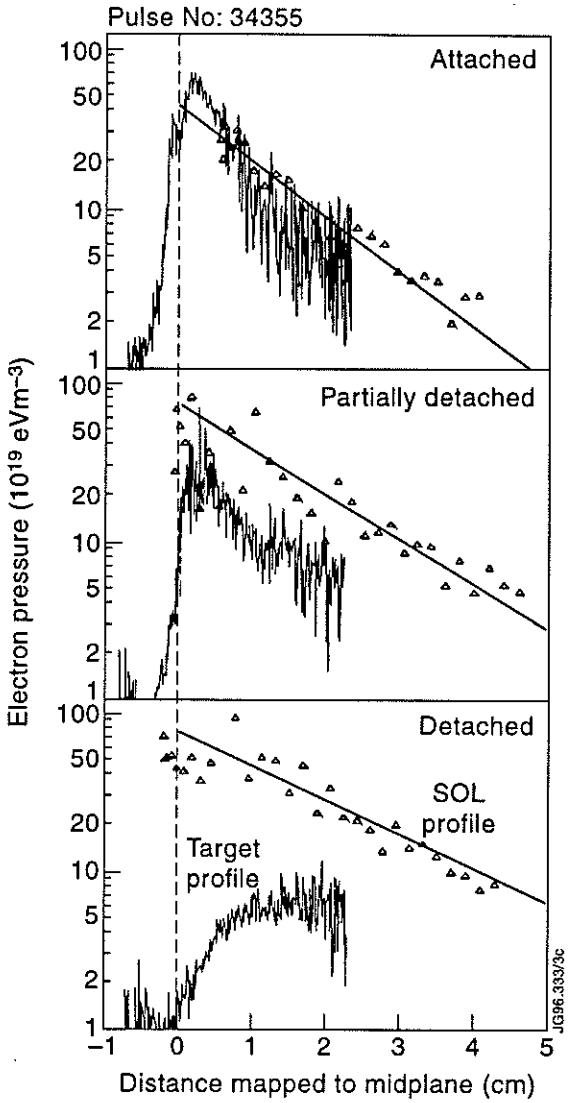

Figure 6: Pressure drop along the scrape-off layer at three different times during an Ohmic density limit experiment. The upstream SOL pressure (triangles and exponential fit) is measured by a reciprocating probe moving in from the top of the machine. The target profiles are measured by fixed Langmuir probes in the target tiles.

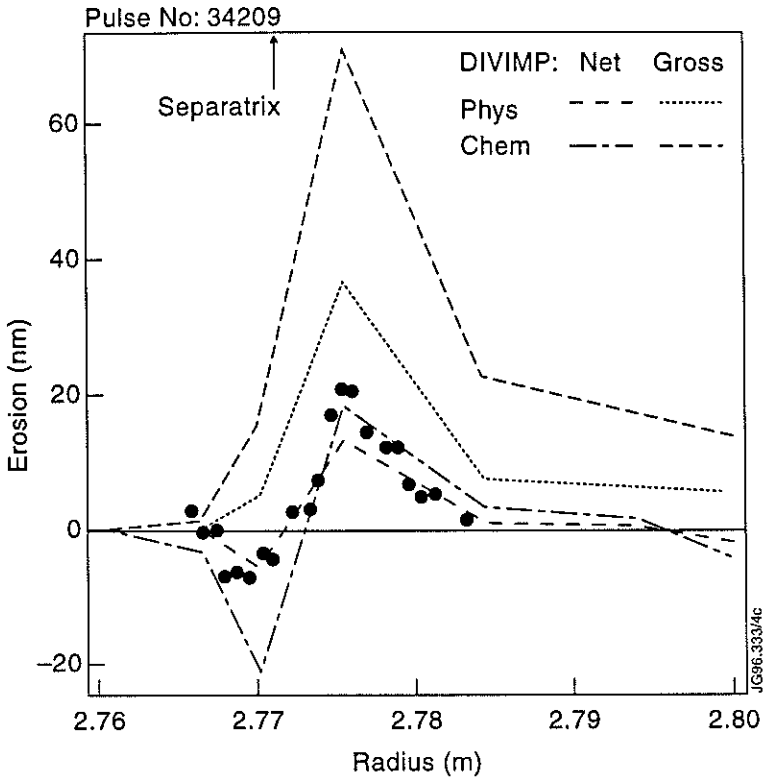

Figure 7: The profile of target erosion for a hot-ion H-mode discharge. The measurement (solid circles) is compared to modelling using the DIVIMP impurity transport code [7]. Good agreement is found only if a significant fraction of the carbon which is chemically sputtered from the surface is redeposited locally.

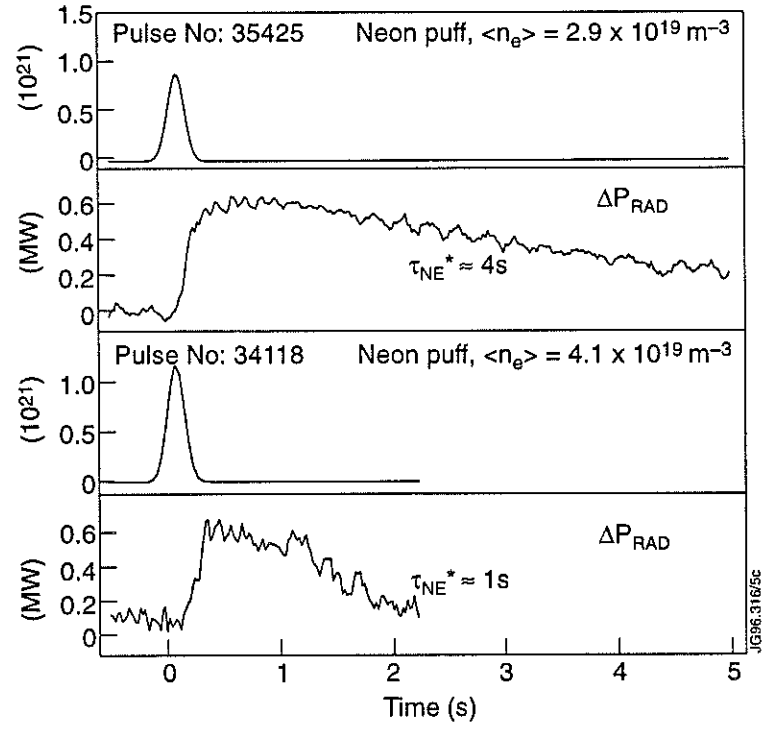

Figure 8: Dependence of the neon exhaust time on the plasma density.

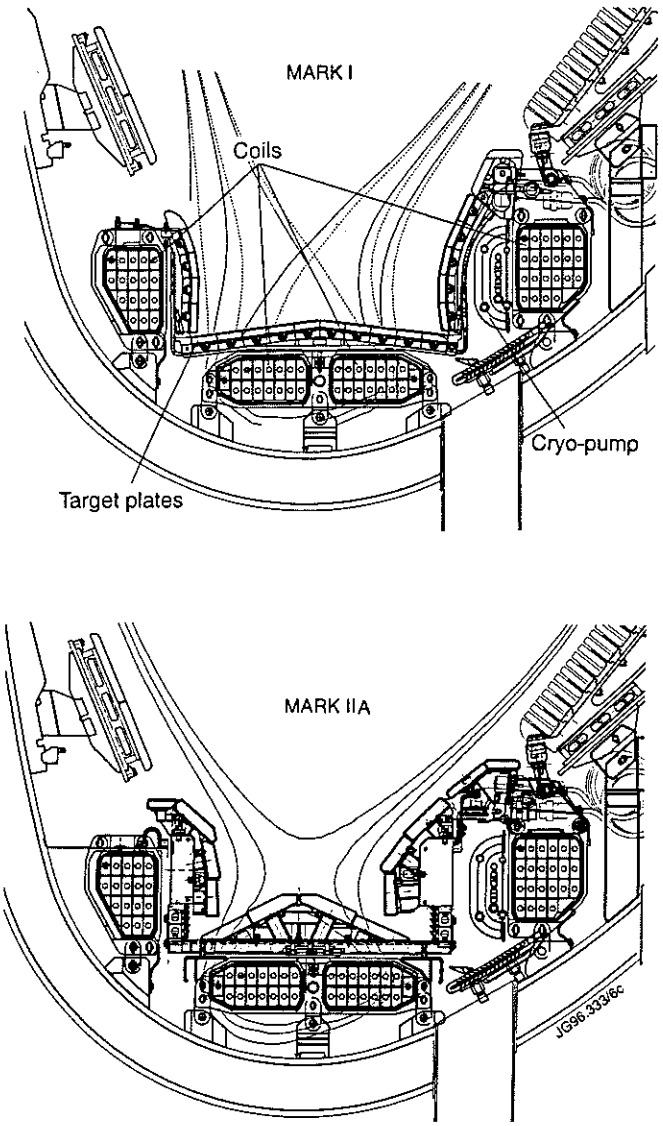

Figure 9: Comparison of the geometry of the JET Mark I and Mark IIA divertors.

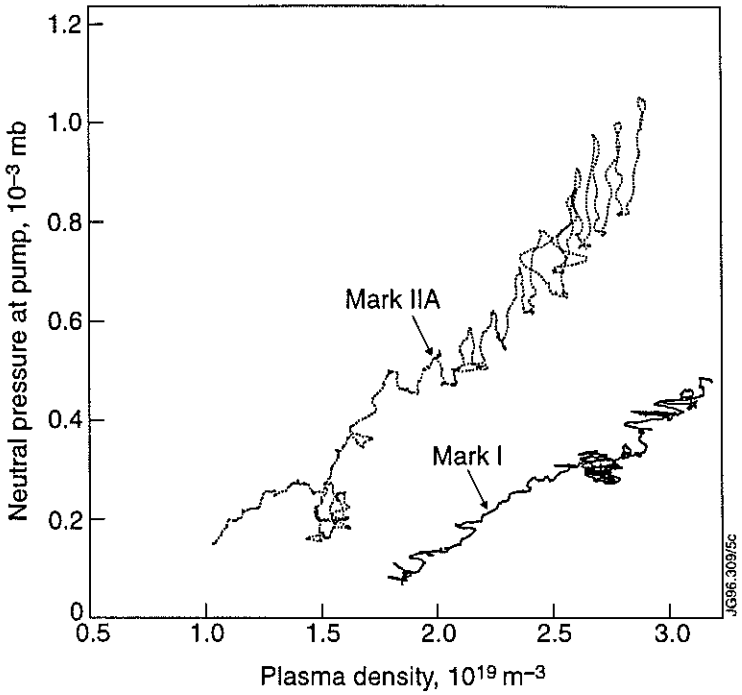

Figure 10: Comparison of the subdivertor pressures and thus of the pumping speeds of the Mark I and Mark IIA divertors as a function of plasma density for two Ohmic discharges.

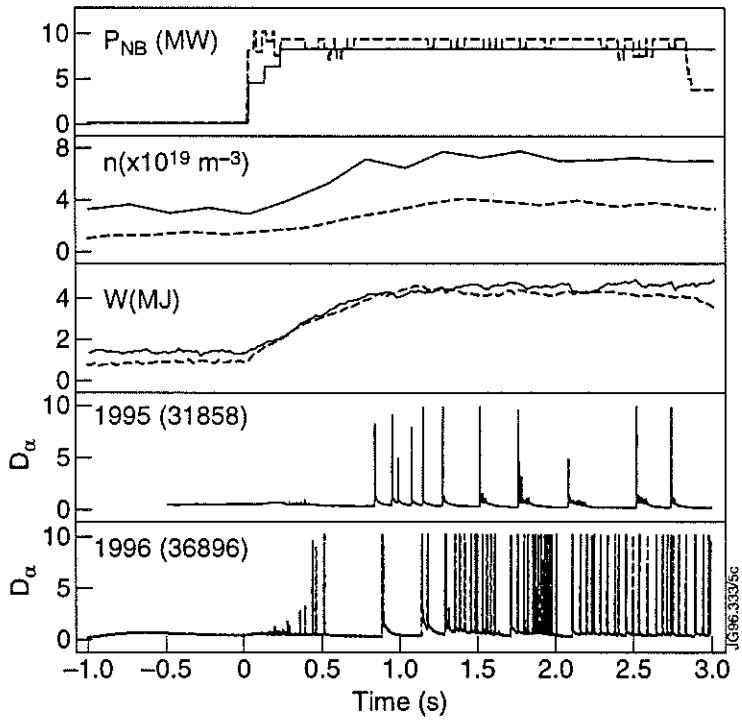

Figure 11: Comparison of two ELMy H-mode discharges, one in the Mark I divertor (solid curves) and one in Mark IIA (dashed curves). Both discharges are at a plasma current of 2.5 MA and a toroidal magnetic field of 2.5 T. Shown are the input neutral beam power, the volume-averaged density, the plasma diamagnetic stored energy, and the D_α emission from the divertor region.

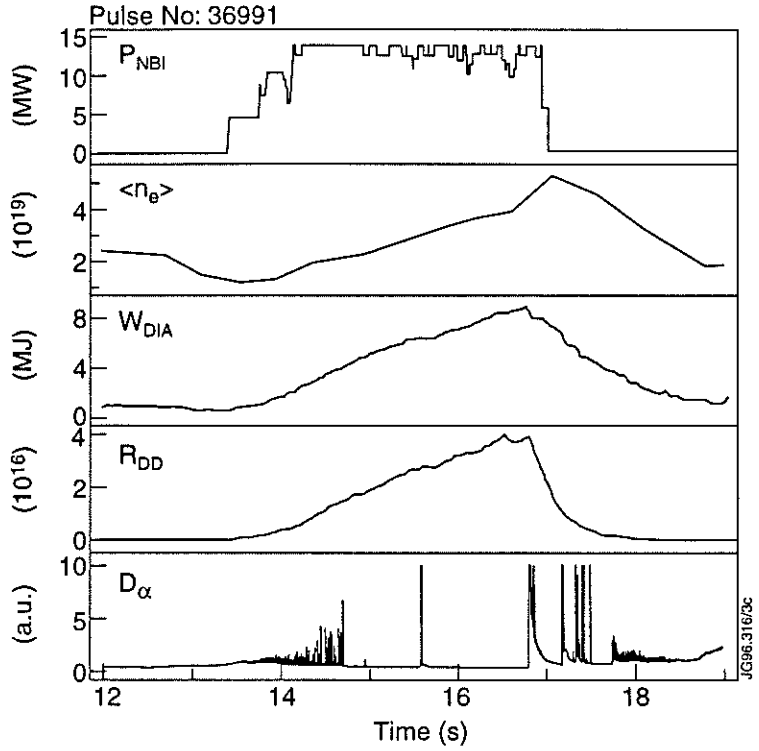

Figure 12: Time traces of an ELM-free H-mode in the Mark IIA divertor. Shown are the input power, the volume-averaged density, the diamagnetic stored energy, the D-D neutron rate, and the D_α emission from the divertor region.

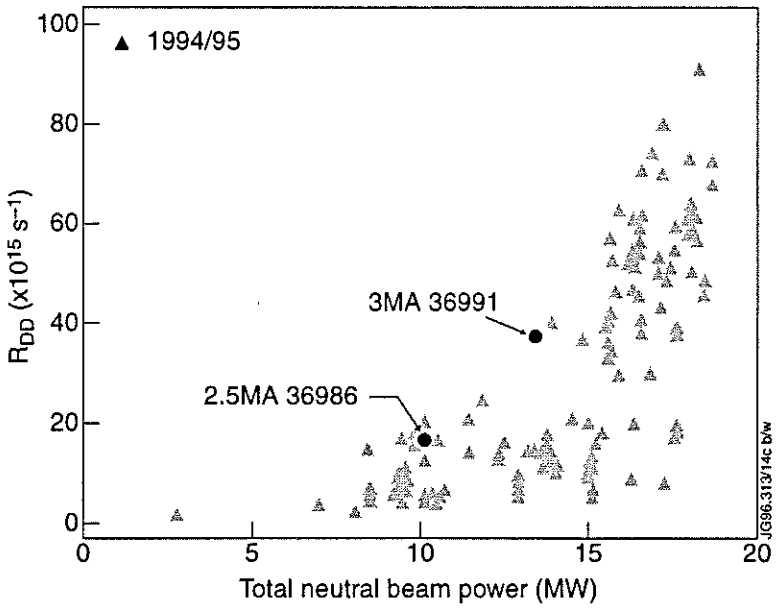

Figure 13: Comparison of the D-D neutron rate of two discharges in the first day of high performance operation with the Mark IIA divertor (circles) and the data from the Mark I campaign (triangles).